Materials Views
www.MaterialsViews.com

ADVANCED
FUNCTIONAL
MATERIALS
www.afm-journal.de

FULL PAPER

# In Situ Formation of Dendrites in Eumelanin Thin Films between Gold Electrodes

*Julia Wünsche, Luis Cardenas, Federico Rosei, Fabio Cicoira, Reynald Gauvin, Carlos F. O. Graeff, Suzie Poulin, Alessandro Pezzella, and Clara Santato**

**Eumelanin is a ubiquitous pigment in the human body, animals, and plants, with potential for bioelectronic applications because of its unique set of physical and chemical properties, including strong UV-vis absorption, mixed ionic/electronic conduction, free radical scavenging and anti-oxidant properties. Herein, a detailed investigation is reported of eumelanin thin films grown on substrates patterned with gold electrodes as a model system for device integration, using electrical measurements, atomic force microscopy, scanning electron microscopy, fluorescence microscopy, and time-of-flight secondary ion mass spectroscopy. Under prolonged electrical biasing in humid air, one can observe gold dissolution and formation of gold-eumelanin nanoaggregates, the assembly of which leads to the formation of dendrites forming conductive pathways between the electrodes. Based on results collected with eumelanins from different sources, a mechanism is proposed for the formation of the nanoaggregates and dendrites, taking into account the metal binding properties of eumelanin. The surprising interaction between eumelanin and gold points to new opportunities for the fabrication of eumelanin-gold nanostructures and biocompatible memory devices and should be taken into account in the design of devices based on eumelanin thin films.**
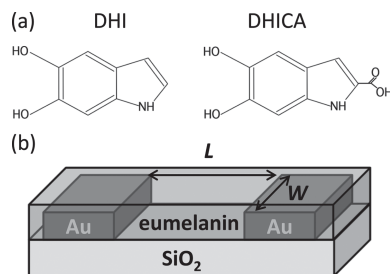
## 1. Introduction

Eumelanin has been the subject of intensive research in biology, biochemistry, and medicine due to its diverse functions in the human body and its involvement in diseases such as melanoma skin cancer and Parkinson's disease.[1–3] In the 1960s and 1970s, after reports on the semiconductor-like behavior of eumelanin pellets, research on eumelanin extended to physics and materials science.[4–7] Nevertheless, the limited solubility and chemical heterogeneity of eumelanin macromolecules, based on 5,6-dihydroxyindole (DHI) and 5,6-dihydroxyindole-2-carboxylic acid (DHICA, **Scheme 1**) building blocks, made its characterization challenging.[8–10] Recent progress in eumelanin thin film processing has created new opportunities for the study of the fundamental and functional properties of eumelanin and its integration into thin film devices.[11–15] Eumelanin is of potential interest for organic bioelectronic applications due to their metal chelation properties,[16] mixed ionic/electronic conduction,[17] broad band UV-vis absorption,[18] free radical scavenging properties,[19] and their intrinsic biocompatibility.[20]

A number of studies have been reported on the preparation and functionalization of coatings based on eumelanin for applications in catalysis, cell imaging, and nerve tissue engineering.[13,20–24] On the other side, only a few studies have been reported on the chemical and physical properties of eumelanin thin films in device structures relevant to bioelectronics. In particular, eumelanin-Au nanoparticle hybrid films have been prepared on electrode surfaces for biosensing.[25,26] A piezoelectric sensor has been functionalized with eumelanin for metal ion sensing.[27] Ambrico et al. studied the memory-like behavior of eumelanin films sandwiched between Au and doped silicon/

J. Wünsche, S. Poulin, Prof. C. Santato
Département de génie physique
École Polytechnique de Montréal
CP 6079, Succursale Centre-Ville, Montréal
Québec H3C 3A7, Canada
E-mail: clara.santato@polymtl.ca
Dr. L. Cardenas, Prof. F. Rosei
INRS-EMT
Université du Quebec
1650 Boul. Lionel Boulet
Varennes, Québec J3X 1S2, Canada
Prof. F. Cicoira
Département de génie chimique
École Polytechnique de Montréal V
CP 6079, Succursale Centre-Ville, Montréal
Québec H3C 3A7, Canada

Prof. R. Gauvin
Department of Mining and Materials Engineering
McGill University
3610 rue University
Montreal, Quebec H3A 0C5, Canada
Prof. A. Pezzella
Department of Chemical Sciences
University of Naples Federico II
Via Cintia 4, 80126 Napoli, Italy
Prof. C. F. O. Graeff
DF-FC, Universidade Estadual Paulista
Av. Eng. Luiz Edmundo Carrijo Coube 14-01
17033-360 Bauru, Brazil

ADVANCED
FUNCTIONAL
MATERIALS
www.afm-journal.de

*Materials Views*
www.MaterialsViews.com

FULL PAPER



**Scheme 1.** a) Main building blocks of the eumelanin macromolecule: 5,6-dihydroxyindole (DHI) and 5,6-dihydroxyindole-2-carboxylic acid (DHICA). b) Planar structure of Au electrodes and eumelanin film used in this work.

indium tin oxide.[28–30] To assess the potential of eumelanin for applications in bioelectronic devices, the properties of eumelanin thin films interfaced with device components, such as metal electrodes, in presence of water and ionic species need to be further explored.

Here we report on the interaction of hydrated eumelanin thin films with gold electrodes in a planar configuration. This geometry represents the first step towards transistor-based sensing devices.[31,32] We observed the in situ formation of Au-eumelanin dendrites, leading to a resistive change in the eumelanin film, and characterized their morphological, chemical, and electrical properties. Our results suggest an active role of eumelanin in Au dissolution and formation of dendrites, based on its metal-binding phenolic hydroxyl groups. The discovery of the interaction between eumelanin and Au in a thin film device structure opens new avenues for the fabrication of Au-eumelanin nanostructures and biocompatible memory devices[33] and emphasize how crucial is the choice of the electrode material in eumelanin-based electronic devices.

## 2. Results

### 2.1. Formation of Au-Eumelanin Nanoaggregates and Dendrites: Morphological and Photoluminescent Properties

Eumelanin films were deposited from dimethyl sulfoxide (DMSO) suspensions onto $SiO_2$ substrates pre-patterned with gold electrodes (Scheme 1). Upon application of 1 V bias between the metal electrodes in air with 90% relative humidity at room temperature, atomic force microscopy (AFM) revealed the formation of nanostructures within the interelectrode region on the timescale of minutes to hours (**Figure 1**a–f). Initially, nanoaggregates (NAs) formed in proximity of the positively biased electrode (Figure 1b). These NAs are made up of Au and most likely also eumelanin, as will be shown below. Prolonged biasing, for a few more minutes, caused the NAs to move towards the negatively biased electrode (Figure 1c). A comparison of the film cross section before (Figure 1a) and after (Figure 1c) biasing reveals a depression at the edge of the positive electrode (Figure 1f). The bright line parallel to the positively biased electrode in Figure 1c is likely an agglomeration of eumelanin and Au. Its position coincides with the initial position of the positive electrode edge. The depression

beyond this line is due to the decomposition of the Au electrode (indicated with ① in Figure 1c). When the NAs reached the edge of the negative electrode, they nucleated and formed dendrite-like structures (indicated with ③ in Figure 1c, see also Figure 1e and Supporting Information S1), which are typical of diffusion-limited aggregation.[34] The growth continues as long as the bias is applied, leading to dendrites extending over the interelectrode region (from the negative to the positive electrode) and beyond (Supporting Information Figure S1). The profile in Figure 1f reveals the typical heights for the newly formed structures: separate NAs (indicated with ②) were up to several tens of nanometer-high, while dendrites (indicated with ③) had a quite uniform height between the electrodes of a sample, typically only 5–10 nm. This height difference suggests that the NAs partially decomposed during dendrite formation.

Conductive AFM measurements showed that the dendrites are highly conductive and in electrical contact with the gold electrodes (**Figure 2**). Charges were injected from the conductive AFM tip into the dendrites only above a certain threshold voltage, thus suggesting the presence of a poorly conductive material on top of the conductive structures, most likely eumelanin-based (Supporting Information Figure S2). The height image in Figure 2 further shows that the dendrites grow higher and larger once they reach the positive electrode since their extension in forward direction is blocked by the electrode.

High resolution scanning electron microscopy images (SEM) and energy-dispersive X-ray spectroscopy (EDS) measurements on the dendrites are shown in **Figure 3**. The EDS spectra (Figure 3e), taken at positions corresponding to those indicated in Figure 3c, and the gold EDS mapping (Figure 3d and Supporting Information Figure S3) clearly indicate that the dendrites have a high gold content. The presence of carbon (originating from eumelanin and the environment), silicon (from the $SiO_2$ substrate), and oxygen (from substrate, eumelanin, and the environment) is also observable in the spectra (Figure 3e).

In Figure 3a, the horizontal bright line included in the upper circle corresponds to the edge of the positive electrode before electrical biasing. The dark regions beyond this line indicate that the nanostructures were formed under dissolution of gold at the electrode edge. The high-resolution images (Figure 3b,c), corresponding to the regions marked with circles in **Figure 4**a, show that the dendrites initially had a porous fine structure (Figure 3b) but became more and more compact during the growth (see the dendrite trunk in Figure 3c). In the initial stage of dendrite growth, many gold-rich dendrite parts were not in direct contact with each other but appeared like equally spaced filaments and nanoparticles (Figure 3b and Supporting Information Figure S4). This suggests that the gold portion of the NAs is surrounded by eumelanin, which affects their assembly.

Fluorescence microscopy provided us with further insight on the nature of the nanostructures formed. In contrast to eumelanin, which has an extremely low fluorescence yield,[35] and large Au particles, Au clusters can be fluorescent.[36,37] A weak emission around 655 nm, attributable to Au clusters of about 25 atoms, was detected after biasing the eumelanin film (Supporting Information Figure S5).[36,38] The fluorescence
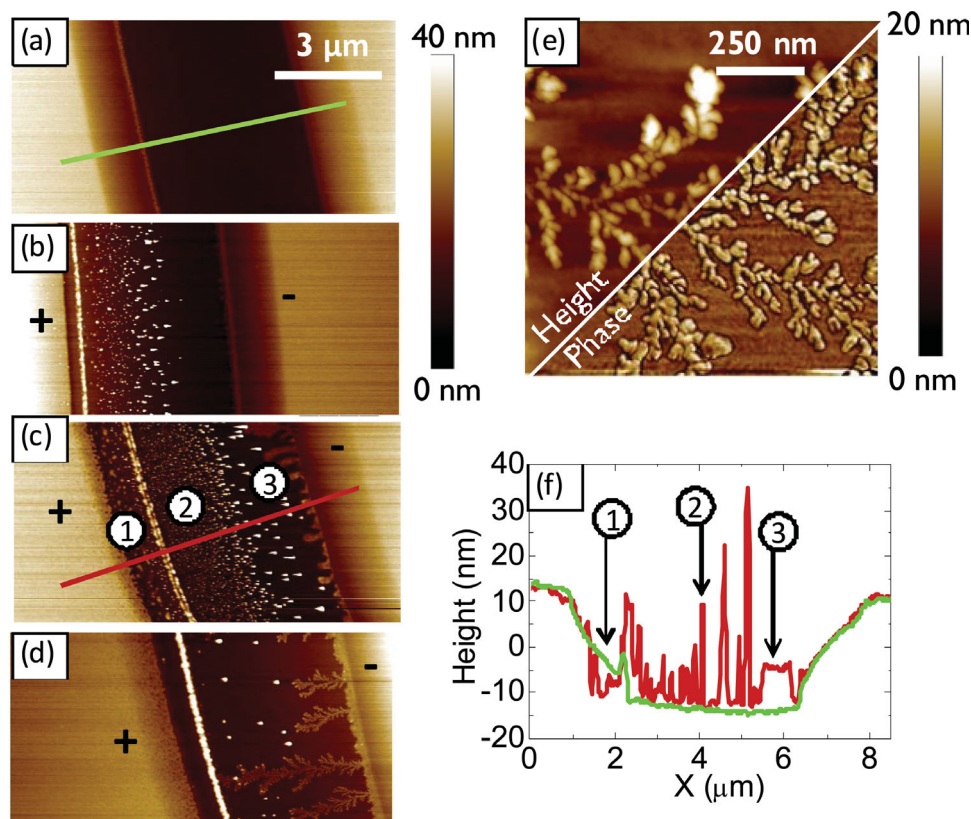
www.MaterialsViews.com

ADVANCED
FUNCTIONAL
MATERIALS
www.afm-journal.de

FULL PAPER

**Figure 1.** AFM images of eumelanin thin films between Au electrodes ($L = 6$ μm) a) before electrical biasing and b–d) after biasing at 1 V for increasing times. Numbers in (c) mark the distinct features of the growth of the nanostructures: ① Decomposition of the positively biased Au electrode, ② NAs moving towards the negatively biased electrode, and ③ dendrite growth. e) AFM height and phase image of dendrite structures. f) Height profile for the sections in (a) (green) and (c) (red).

signal disappeared after removing eumelanin by exposing the sample to a 1-h-long UV-ozone treatment (Supporting Information Figure S6). A possible interpretation of this result is that eumelanin stabilizes the Au clusters and that the clusters aggregate to form relatively large, non-fluorescent Au particles in the absence of eumelanin.
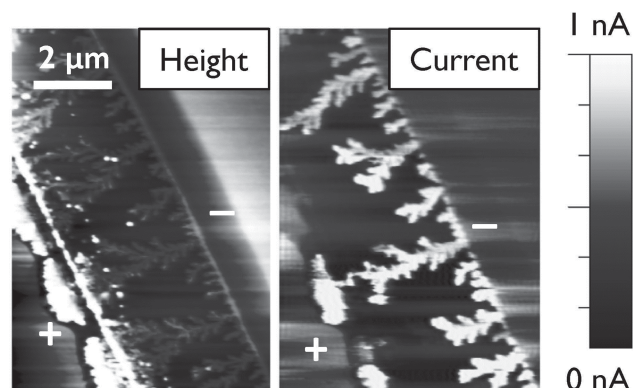


**Figure 2.** AFM and corresponding conductive AFM image of the dendrite-like structures extending from the negative to the positive electrode. The voltage applied to the AFM tip was −10 V.

## 2.2. Resistive Change in Eumelanin Films on Au Electrodes

We carried out transient measurements of the electrical current between the Au electrodes during the formation of nanostructures (Figure 4a). The rapidly decreasing current during the first few minutes was likely dominated by ionic currents (capacitive currents), in agreement with recent works suggesting the presence of mobile ions (such as $H^+$ and $OH^-$) in eumelanin films.[17,29] It was followed by a slowly decreasing current including contributions from electrochemical reactions and, possibly, purely electronic charge transport. After several minutes to a few hours of biasing, a sudden increase of current over 3–6 orders of magnitude was observed. The onset of this increase corresponded to the first dendrite connecting the two electrodes, as indicated by AFM images (Supporting Information Figure S7). The shape of the current transient after this first increase varied from sample to sample (Supporting Information Figure S8). However, some features were typical: the current initially alternates between high and low values; the further increase occurred in discrete steps or under strong fluctuations, and the current saturated around $10^{-2}$–$10^{-3}$ mA (for an electrode geometry with $L = 6$ or 10 μm, $W = 2$ or 4 mm with a film thickness about 30 nm; see Figure 4a,b, and Supporting Information Figure S8).
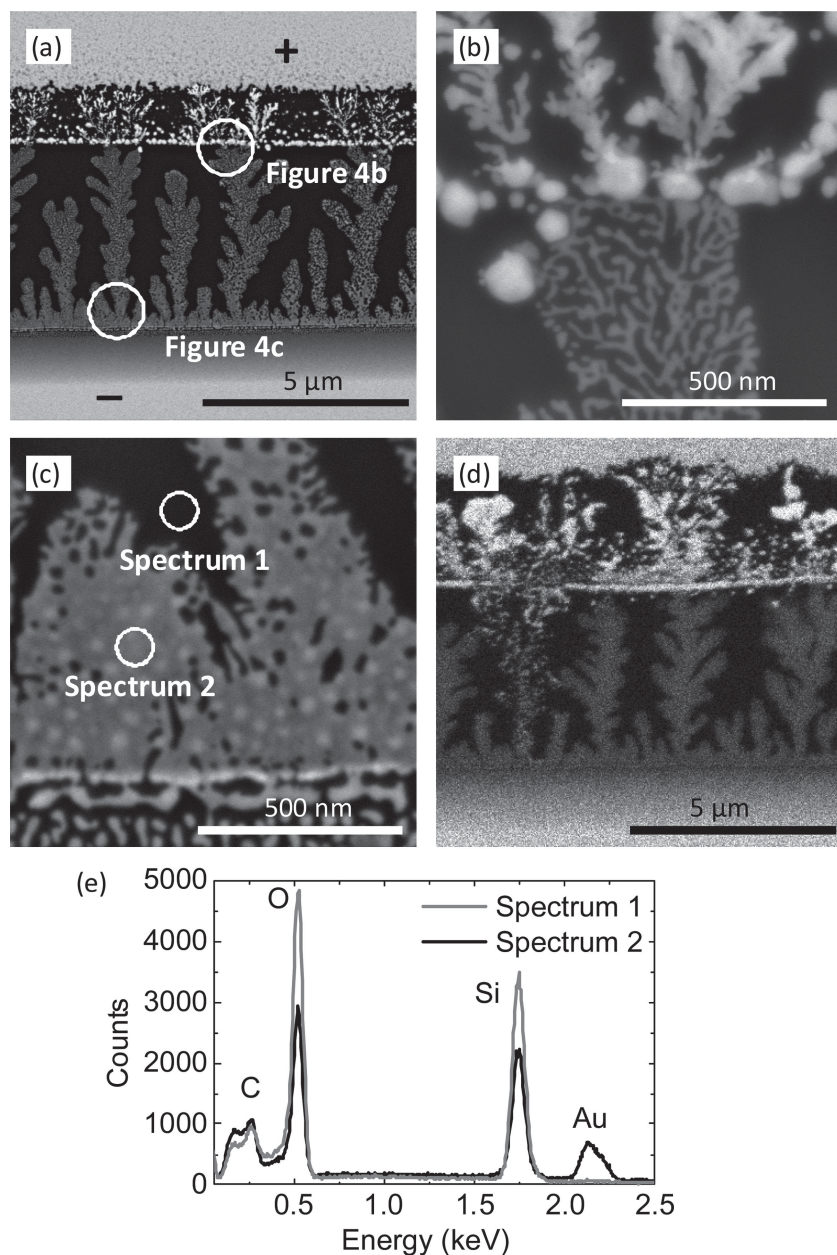
**Figure 3.** a) SEM images of the dendrites growing on the eumelanin film between the Au electrodes using the backscattered electron signal (BSE). b,c): High-resolution SEM-BSE images taken at positions similar to those marked in (a). d) Mapping of the gold distribution based on the EDS signal. e) EDS spectra taken at positions similar to those marked in (c).

The fluctuations in the electrical current are due to the growth of an increasing number of conductive dendrites between the electrodes and to the continuous evolution of the contact between the dendrite and the positive electrode, including also a possible breaking of the contact. In some devices, the variation of the current between discrete values of conductance (Figure 4b,c) reminds of the quantized conductance of atom-sized conductors, which is well studied for gold.[39,40] The conductance of the sample of Figure 4b,c preferably varied between multiples of $G_0/4$, where $G_0 = 2e^2/h = 77.48$ µS, the quantum of conductance. This could be an indication of both the atom-size

of the contact between the dendrite and the electrode and the organic-inorganic hybrid character of the eumelanin-Au dendrites (since conductance values smaller than $G_0$ were found).[40] However, the current steps we observed varied from sample to sample and were not always well defined, which should be due to the hybrid character of the eumelanin-Au dendrites and their complex environment.

The highly conductive state was stable up to 0.55 V (Figure 4d). At 0.60 V and above, current fluctuations occurred in the current vs time plot, caused by breaking and creating contacts between the dendrites and the electrode, likely due to electrochemical reactions (Supporting Information Figure S4b). Within the stability window from −0.5 V to 0.5 V, the samples displayed highly linear I–V characteristics, even at a conductance below $G_0$ (Supporting Information Figure S9).

## 2.3. Effect of Electrical Bias, Sample Hydration, and Processing Solvent on the Formation of Nanoaggregates and Dendrites

We investigated the conditions that promote the formation of Au-eumelanin nanostructures between planar Au electrodes. NAs formed upon application of an electrical bias of 0.7 and 1 V, whereas 0.3 and 0.5 V were not sufficient (Supporting Information Figure S10). This is in agreement with the voltage-step measurement reported in Figure 6d and suggests that the electrochemical reactions leading to the formation of NAs set in for biases larger than 0.55 V.

The presence of water in the film was crucial for the formation of NAs. When eumelanin was deposited from anhydrous DMSO suspensions and sample processing and electrical characterization were conducted under dry nitrogen atmosphere ($H_2O$ and $O_2$ content <0.1 ppm), no NA formation could be observed and the eumelanin film was not conductive enough to yield currents above noise level.

Another requirement for the formation of dendrites was the presence of traces of the low- volatility solvent DMSO that leaves the film in a gel-like state, enhancing the mobility of the NAs on the film surface. After solvent removal by heat treatment, NAs still formed under electrical bias but they were confined to a small region close to the positive electrode (Supporting Information Figure S11). The dendrite growth and the highly conductive state were also reproduced with eumelanin films deposited from dimethyl formamide (DMF) suspensions indicating that the phenomenon is not specific to suspensions of eumelanin in DMSO (Supporting Information Figure S12).
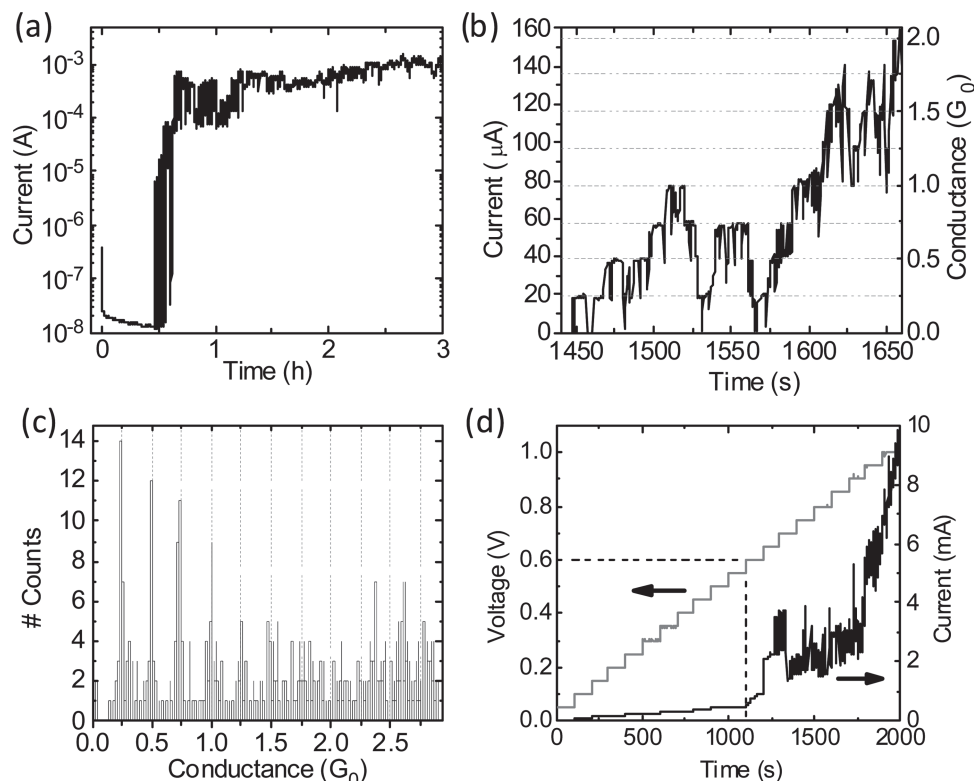
www.MaterialsViews.com

ADVANCED
FUNCTIONAL
MATERIALS
www.afm-journal.de

FULL PAPER

**Figure 4.** a) Transient current measurement for a eumelanin film between Au electrodes ($L = 10$ μm, $W = 2$ mm, applied voltage 1 V) at 90% relative humidity. The sample was left hydrating for 24 h before biasing. b) Example for the resistive change of eumelanin films with Au-eumelanin dendrites between states of discrete resistance ($L = 6$ μm, $W = 4$ mm, applied voltage 1 V). c) Conductance histogram corresponding to (b). d) Voltage-step measurement of an Au-eumelanin-Au structure ($L = 6$ μm, $W = 4$ mm). The sample was biased at 1 V beforehand to attain the highly conductive state. The dashed lines separate the region of linear $I$–$V$ characteristics from the region of electrochemical reactions.

## 2.4. Investigation of Eumelanins from Different Sources

To investigate the mechanism of Au dissolution and dendrite formation, we tested eumelanins with different chemical compositions, obtained by different synthetic routes or as natural eumelanin.[9,41] More precisely, we investigated: commercial eumelanin (Sigma Aldrich) obtained by the oxidation of tyrosine (from now on indicated as *Sigma melanin*), used for all experiments presented above; eumelanin obtained by the non-enzymatic polymerization of DHICA in aqueous solution (*DHICA melanin*); the *DHICA monomer* without further polymerization;[42] eumelanin obtained by the oxidation of 3,4-dihydroxy-L-phenylalanine (dopa) in DMSO solution (*DMSO melanin*);[11] *DMSO melanin* treated with NaOH; natural eumelanin extracted from Sepia officinalis (*Sepia melanin*).[41] The results are summarized in **Table 1** and described in detail in the Supporting Information (Figures S13-S17). In particular, we quantified the Cl⁻ concentration in the different eumelanins by nuclear activation analysis (NAA, Table 1), because halides, especially Cl⁻, are known to enable the electrochemical oxidation and dissolution of Au.[43–45] Br⁻ and I⁻ concentrations were negligible compared to Cl⁻ and are therefore not listed.

*Sigma melanin* and *Sepia melanin* both led to sudden resistive change, although it was difficult to image the dendrites for *Sepia melanin,* due to a very inhomogeneous substrate coverage. *Sepia melanin* had the highest Cl⁻, amongst the eumelanins investigated, followed by *Sigma melanin*, whereas all other eumelanins had much lower Cl⁻ concentrations.

*DHICA melanin* clearly interacted with the Au electrodes under electrical bias, as evident from the strong accumulation at the positive electrode (Supporting Information Figure S14). However, no NAs or dendrites were formed, possibly related to a high degree of polymerization and limited substrate coverage.

**Table 1.** Summary of results from electrical measurements, AFM/optical microscopy, and nuclear activation analysis of Cl⁻ concentration on eumelanins obtained from different sources.

| Sample | Resistive change | Nanostructures | [Cl] [mg g⁻¹] |
|---|---|---|---|
| Sigma melanin | Yes | Dendrites | 7.0 ± 0.3 |
| Sepia melanin | Yes | Difficult to image due to film inhomogeneity | 64.1 ± 2.6 |
| DHICA melanin | No | Strong accumulation at positive electrode | 0.28 ± 0.02 |
| DHICA monomer | Yes | Dendrites | 0.20 ± 0.02 |
| DMSO melanin | No | No | 0.34 ± 0.02 |
| NaOH-treated DMSO melanin | Yes | Dendrites | Not measured |

ADVANCED
FUNCTIONAL
MATERIALS
www.afm-journal.de

Materials
Views
www.MaterialsViews.com

Therefore, we also prepared films directly from the *DHICA monomer*, which was easier to process. In this case, we observed dendrite formation and resistive change (Supporting Information Figure S15).

Films of *DMSO melanin*, having a slightly higher Cl⁻ content than the *DHICA monomer* and *DHICA melanin*, did not seems to react with the Au electrodes or yield any other significant change under electrical bias (Supporting Information Figure S16). As recently discovered, *DMSO melanin* differs in molecular structure from *Sigma* and *DHICA melanin* by the incorporation of sulfonate groups–$SO_2CH_3$, primarily binding to the phenolic hydroxyl groups.[41] The latter are known to be metal chelation sites of eumelanin.[16,46] Only after removal of the sulfonate groups by treatment with NaOH,[41] *DMSO melanin* also led to dendrite formation and resistive changes (Supporting Information Figure S17). This result is a strong indication for the active participation of the eumelanin metal binding sites, particularly phenolic hydroxyl groups, in the process of Au dissolution and the subsequent formation of nanostructures.

To gain further insight into the chemical properties of the eumelanin-Au interface, time-of-flight secondary ion mass spectroscopy (ToF-SIMS) measurements were conducted on selected eumelanin-Au samples after electrical biasing. Dendrites could be located only if they were exceptionally large (about 100 nm in height and 1 µm in width) as in the sample of *Sigma melanin* in Supporting Information Figure S18. In this case, ToF-SIMS indicated the presence of Cl⁻ in the dendrite region. A preliminary analysis of the high-mass region of the ToF-SIMS revealed the presence of a number of ionic complexes of the type $[(M-H_v)_x-Au_yCl_z]^{-/-/+/++}$ (M = DHI monomer, v = {0,2}, x = {1,2,3}, y = {1,2}, z = {0,1}). A chemometric analysis of the ToF-SIMS spectra is underway to get more insights into complex formation between eumelanin, Au, and Cl⁻.

## 3. Discussion

AFM and SEM images show that the positively biased Au electrode in contact with the hydrated eumelanin film is partially dissolved upon application of an electrical bias above 0.55 V. Details of the Au dissolution and the role of Cl⁻, present in all eumelanin samples, sometimes only in trace amounts, require further investigation. We hypothesize that the Au dissolution is due to the electrochemical oxidation of Au enabled by Cl⁻[44] and that eumelanin with active phenolic hydroxyl groups, which act as metal binding sites, strongly enhances the Au dissolution. This hypothesis is supported by the results obtained on eumelanins with low Cl⁻ concentrations, having different molecular structures, namely *DHICA melanin*, *DHICA monomer* as well as untreated, and NaOH-treated *DMSO melanin*. The presence of a eumelanin with active phenolic hydroxyl groups was required to obtain dendrite growth and resistive changes at low Cl⁻ concentrations. The eumelanin analogue polydopamine and the eumelanin precursor dopa have been recognized as efficient binding and reducing agents for Au cations, which was ascribed to their phenolic hydroxyl groups.[23,26,47] Understanding the (electro-)chemical reactions leading to eumelanin-enhanced dissolution of Au is of significant interest. Nevertheless, at present, any conclusion

supported by experimental evidence is challenged by the difficulties in locally probing the chemical compounds formed at the positive electrode and in predicting (electro-)chemical reactions in a hydrated solid-state environment with unknown local pH. Based on the process suggested for the halide-catalyzed dissolution of Au in acetonitrile,[44] we suggest that Cl⁻ adsorbs on the surface of the positively biased Au electrode and enables the electrochemical oxidation of Au by the displacement of water and under formation of $AuCl_x$. Eumelanin binds and partly reduces $Au_x^+$ ions from $AuCl_x$ complexes mainly through its phenolic hydroxyl groups. This leads to the release of Cl⁻, which subsequently can facilitate the electrochemical oxidation of further Au atoms. Cl⁻ could thus have a purely catalytic role, when present at low concentrations.

Polydopamine and dopa have been exploited as reducing agents for the formation of Au nanoparticles in $HAuCl_4$ solution.[23,26,47] Along this line of thought, eumelanin can be expected to promote the formation of Au nanoparticles in our case. The NAs we observed are likely to contain Au cluster and/or nanoparticles, which is supported by fluorescence measurements.

The migration of NAs to the negative electrode indicates their residual positive charge. The drift and the residual charge of the NAs prevent their assembly to larger structures before arrival at the negative electrode. Once in contact with the negative electrode (directly or via dendrite), the NAs are electrochemically reduced, which is likely to break up some of the eumelanin-Au complexes. The NAs nucleate at the negative electrode and dendrites start to grow from the negative towards the positive electrode. This direction of growth is in agreement with the working principle of electrochemical metallization cells.[33] SEM images suggest that eumelanin is an integral part of the initial dendrite structure but that the Au parts of the dendrites become more and more connected as the growth continues. Eumelanin has been reported to chemisorb on negatively biased Au surfaces, permitting efficient charge transfer,[25,48] which favors the charge transport along the Au-eumelanin dendrites.

The conductive path created by the dendrites and their continuously evolving contact with the positive electrode lead to sudden changes in conductance, similar to resistive switching memory devices based on electrochemical metallization.[33] Such devices are composed of a solid electrolyte layer, as well as one electrochemically active, where faradic processes take place, and one inert metal counter electrode. By reversing the bias, the devices can be switched between the on- and off-state. Due to its chemical properties, Au is usually used as the inert electrode.[33] In this work, Au forms the electrochemically active and counter electrodes and eumelanin the solid electrolyte, playing an active role in the Au dissolution. We suggest that, in principle, biocompatible eumelanin-Au based memory devices could be built by exchanging the counter Au electrode for a conductive material that is non-reactive with eumelanin.

Our findings on the interaction of Au, eumelanin, and Cl⁻ shed light on previously reported results about the electrical properties of eumelanin films in presence of Au electrodes. Ambrico et al. reported memory switching in vertical Au/eumelanin/p-Si and Au/eumelanin/indium tin oxide structures, claiming the absence of metallic nanoclusters in the

eumelanin film without however reporting experimental evidence.[28–30] Au electrodes were also used in several other works to characterize the conductivity of hydrated eumelanins.[17,20,49] In particular, Bettinger et al. reported negligible contact resistance for hydrated films of *Sigma melanin* with Au electrodes.[20] Our results suggest that electrode materials alternative to Au, such as Pt, graphene, carbon nanotubes, or conductive polymers, should be considered to study the intrinsic properties of eumelanin.

## 4. Conclusion

We showed that hydrated eumelanin films between Au electrodes under electrical bias lead to the formation of Au-eumelanin NAs and dendrites in the interelectrode region. This phenomenon was observed with eumelanins from different sources, as long as they have active phenolic hydroxyl groups. We suggest that the dissolution of the Au electrode is enabled by low amounts of $Cl^-$, present in eumelanins, and that the reducing and metal binding ability of eumelanin is responsible for a strong enhancement of Au dissolution and the formation of NAs. The interaction between eumelanin and Au can potentially be exploited for the *in situ* formation of Au-eumelanin nanostructures and biocompatible resistive switching memory devices. Moreover, the interaction between Au and eumelanin has to be taken into account for the design of bioelectronic devices based on eumelanin thin films.

## 5. Experimental Section

*Materials and Sample Preparation*: Synthetic eumelanin (Sigma Aldrich, *Sigma melanin*) was dissolved in dimethyl sulfoxide (DMSO, Sigma Aldrich, purity >99.9%) to yield a 15 mg mL$^{-1}$ suspension, unless otherwise stated. The suspension was stirred for 30 min and filtered. The substrates were silicon wafers with 200 nm thermal $SiO_2$ and 30-nm-thick Au electrodes on a 4-nm-thick adhesion layer of Cr, deposited by e-beam evaporation and patterned by photolithography. Before film deposition, substrates were cleaned in an ultrasonic bath with acetone, isopropanol, and de-ionized water, followed by 20 min UV-ozone treatment. Eumelanin suspension is spin-coated onto the substrate at 1000 rpm for 2 min followed by 4000 rpm for 30 s. For a control experiment, dimethylformamide (Caledon Laboratories, purity >99.8%) was used instead of DMSO. *DHICA* was synthesized according to the procedure reported in the literature.[42] For non-enzymatic polymerization, *DHICA* was dissolved in distilled water (12.5 mM). Oxygen was bubbled through the solution for 20 min, followed by exposure to ammonia vapors for further 20 min. Finally, the solution was kept under stirring for another 4 h in air. The *DHICA* polymer was extracted by lyophilization. *DMSO melanin* was synthesized and part of it was treated with NaOH according to the procedures described in the literature.[41] *Sepia melanin* was purchased from Sigma Aldrich. The *DHICA monomer*, *DHICA melanin*, *Sepia*, and *DMSO melanin* were dissolved in DMSO (15 mg mL$^{-1}$) and spin-coated on the same substrates and with the same parameters as *Sigma melanin*. *DMSO melanin* treated with NaOH was deposited by drop casting due to its limited solubility in DMSO.

*Sample Characterization*: Current transients and current-voltage curves were measured with a semiconductor parameter analyzer (Agilent B1500A) or software-controlled source/measure unit (Agilent B2902A). Measurements were taken in air with a controlled humidity of 90% after at least 1 h time to hydrate the eumelanin film, unless otherwise

stated. W or Pt probes were used to contact the Au electrodes. AFM measurements were taken with a Dimension 3100 (Digital Instruments) with Si probes (tip radius <10 nm, spring constant 20–100 N m$^{-1}$) in Tapping mode. Images were analysed with Nanoscope Analysis from Bruker. For conductive AFM measurements, a Pt cantilever (constant force <6 nN) was used. A voltage of −10 V was applied between the tip and the Au electrodes on the sample.

SEM measurements were conducted with a Hitachi SU–8000 cold field emission scanning electron microscope combined with a silicon drift detector provided by Oxford Instruments for EDS. Imaging was performed at 5 keV with a through the lens (TTL) backscattered electron (BSE) detector. Most images were taken in BSE mode, since the BSE signal is more sensitive to the chemical composition of the sample than the secondary electron signal. Photoluminescence spectra and images were obtained with a hyperspectral imaging system (PARISS, LightForm Inc), using the (550 ± 10) nm emission of a X-Cite Series 120 short arc lamp. ToF-SIMS measurements were conducted with an ION-TOF SIMS IV using a $Bi_1$ source at 15 kV and 0.7 pA for spectral measurements and a $Bi_3^{++}$ source at 25 kV and 0.013 pA for imaging (both with 200 μs cycle time). The primary ion dose was limited to $1 \times 10^{13}$ ions cm$^{-2}$. Spectra were recorded in Bunch mode using a 19.9 ns primary ion pulse to provide a mass resolution (m/$\Delta$m) >8000 on $^{29}$Si. Images were recorded in Burst mode, in which the lens magnification is set to zero to provide both high lateral resolution of <300 nm and high mass resolution >5000 simultaneously. Nuclear activation analysis was performed with a SLOWPOKE nuclear reactor (Atomic Energy of Canada Limited) and a Ge semiconductor gamma-ray detector (Ortec, GEM55185). The samples were irradiated for 600 s at a thermal neutron flux of $5.4 \times 10^{11}$ cm$^{-2}$ s$^{-1}$. Gamma rays were detected after 120 s for 600 s at a distance of 35 mm.

## Supporting Information

Supporting Information is available from the Wiley Online Library or from the author.

## Acknowledgements

[1] G. Prota, *Melanins and Melanogenesis*, Academic Press, San Diego **1992**.

[2] P. A. Riley, *Int. J. Biochem. Cell Biol.* **1997**, *29*, 1235–1239.

[3] H. Fedorow, F. Tribl, G. Halliday, M. Gerlach, P. Riederer, K. L. Double, *Prog. Neurobiol.* **2005**, *75*, 109–124.

[4] H. Longuet-Higgins, *Arch. Biochem. Biophys.* **1960**, *86*, 231–232.

[5] A. Pullman, B. Pullman, *Biochim. Biophys. Acta* **1961**, *54*, 384–385.

[6] J. E. McGinness, *Science* **1972**, *177*, 896–897.

[7] J. McGinness, P. Corry, P. Proctor, *Science* **1974**, *183*, 853–855.

[8] M. d'Ischia, A. Napolitano, A. Pezzella, *Eur. J. Org. Chem.* **2011**, *2011*, 5501–5516.

[9] M. R. Chedekel, A. B. Ahene, L. Zeise, *Pigm. Cell Res.* **1992**, *5*, 240–246.

[10] M. D'Ischia, A. Napolitano, A. Pezzella, P. Meredith, T. Sarna, *Angew. Chem., Int. Ed.* **2009**, *48*, 3914–3921.

[11] S. N. Dezidério, C. A. Brunello, M. I. N. da Silva, M. A. Cotta, C. F. O. Graeff, *J.Non-Cryst. Solids* **2004**, *338-340*, 634–638.

[12] J. P. Bothma, J. de Boor, U. Divakar, P. E. Schwenn, P. Meredith, *Adv. Mater.* **2008**, *20*, 3539–3542.

[13] H. Lee, S. M. Dellatore, W. M. Miller, P. B. Messersmith, *Science* **2007**, *318*, 426–430.

[14] M. Abbas, F. D'Amico, L. Morresi, N. Pinto, M. Ficcadenti, R. Natali, L. Ottaviano, M. Passacantando, M. Cuccioloni, M. Angeletti, R. Gunnella, *Eur. Phys. J. E: Soft Matter Biol. Phys.* **2009**, *28*, 285–291.

[15] F. Bloisi, A. Pezzella, M. Barra, F. Chiarella, A. Cassinese, L. Vicari, *J. Appl. Phys.* **2011**, *110*, 026105.

[16] L. Hong, J. D. Simon, *J. Phys. Chem. B* **2007**, *111*, 7938–7947.

[17] A. B. Mostert, B. J. Powell, F. L. Pratt, G. R. Hanson, T. Sarna, I. R. Gentle, P. Meredith, *Proc. Natl. Acad. Sci. USA* **2012**, *109*, 8943–8947.

[18] A. Pezzella, A. Iadonisi, S. Valerio, L. Panzella, A. Napolitano, M. Adinolfi, M. d'Ischia, *J. Am. Chem. Soc.* **2009**, *131*, 15270–15275.

[19] T. Sarna, *Biochim. Biophys. Acta* **1986**, *883*, 162–167.

[20] C. J. Bettinger, J. P. Bruggeman, A. Misra, J. T. Borenstein, R. Langer, *Biomaterials* **2009**, *30*, 3050–3057.

[21] H. Lee, J. Rho, P. B. Messersmith, *Adv. Mater.* **2009**, *21*, 431–434.

[22] F. Bernsmann, V. Ball, F. Addiego, A. Ponche, M. Michel, J. J. de A. Gracio, V. Toniazzo, D. Ruch, *Langmuir* **2011**, *27*, 2819–2825.

[23] W. Qu, S. Wang, Z. Hu, T. Cheang, Z. Xing, X. Zhang, A. Xu, *J. Phys. Chem. C* **2010**, *114*, 13010–13016.

[24] M. E. Lynge, R. van der Westen, A. Postma, B. Städler, *Nanoscale* **2011**, *3*, 4916–4928.

[25] A. González Orive, D. Grumelli, C. Vericat, J. M. Ramallo-López, L. Giovanetti, G. Benitez, J. C. Azcárate, G. Corthey, M. H. Fonticelli, F. G. Requejo, A. Hernández Creus, R. C. Salvarezza, A. G. Orive, *Nanoscale* **2011**, *3*, 1708–1716.

[26] F. Li, L. Yang, C. Zhao, Z. Du, *Anal. Methods* **2011**, *3*, 1601.

[27] G. S. Huang, M.-T. Wang, C.-W. Su, Y.-S. Chen, M.-Y. Hong, *Biosens. Bioelectron.* **2007**, *23*, 319–325.

[28] M. Ambrico, A. Cardone, T. Ligonzo, *Org. Electron.* **2010**, *11*, 1809–1814.

[29] M. Ambrico, P. F. Ambrico, A. Cardone, T. Ligonzo, S. R. Cicco, R. Di Mundo, V. Augelli, G. M. Farinola, *Adv. Mater.* **2011**, *23*, 3332–3336.

[30] M. Ambrico, P. F. Ambrico, T. Ligonzo, a. Cardone, S. R. Cicco, A. Lavizzera, V. Augelli, G. M. Farinola, *Appl. Phys. Lett.* **2012**, *100*, 253702.

[31] P. Meredith, T. Sarna, *Pigm. Cell Res.* **2006**, *19*, 572–594.

[32] R. M. Owens, G. G. Malliaras, *MRS Bulll.* **2010**, *35*, 449–456.

[33] R. Waser, R. Dittmann, G. Staikov, K. Szot, *Adv. Mater.* 21, 2632–2663.

[34] T. A. Witten, *Phys. Rev. Lett.* **1981**, *47*, 1400.

[35] J. M. Gallas, M. Eisner, *Photochem. Photobiol.* **1987**, *45*, 595–600.

[36] C. V. Durgadas, C. P. Sharma, K. Sreenivasan, *Analyst* **2011**, *136*, 933–940.

[37] W. Lu, W.-M. Kwok, C. Ma, C. T.-L. Chan, M.-X. Zhu, C.-M. Che, *J. Am. Chem. Soc.* **2011**, *133*, 14120–14135.

[38] C.-A. J. Lin, T.-Y. Yang, C.-H. Lee, S. H. Huang, R. A. Sperling, M. Zanella, J. K. Li, J.-L. Shen, H.-H. Wang, H. Yeh, W. J. Parak, W. H. Chang, *ACS Nano* **2009**, *3*, 395–401.

[39] N. Agraït, A. L. Yeyati, J. M. van Ruitenbeek, *Phys. Rep.* **2003**, *377*, 81–279.

[40] S. Csonka, a. Halbritter, G. Mihály, E. Jurdik, O. Shklyarevskii, S. Speller, H. van Kempen, *Phys. Rev. Lett.* **2003**, *90*, 4–7.

[41] E. S. Bronze-Uhle, A. Batagin-Neto, P. H. P. Xavier, N. I. Fernandes, E. R. de Azevedo, C. F. O. Graeff, *J. Mol. Struct.* **2013**, *1047*, 102–108.

[42] R. Edge, M. D'Ischia, E. J. Land, A. Napolitano, S. Navaratnam, L. Panzella, A. Pezzella, C. a Ramsden, P. a Riley, *Pigm. Cell Res.* **2006**, *19*, 443–450.

[43] R. P. Frankenthal, *J. Electrochem. Soc.* **1982**, *129*, 1192.

[44] R. Kissner, *J. Electroanal. Chem.* **1995**, *385*, 71–75.

[45] C.-C. Yu, Y.-C. Liu, K.-H. Yang, C.-C. Li, C.-C. Wang, *Mater. Chem. Phys.* **2011**, *125*, 109–112.

[46] J. Stainsack, A. S. Mangrich, C. M. B. F. Maia, V. G. Machado, J. C. P. dos Santos, S. Nakagaki, *Inorg. Chim. Acta* **2003**, *356*, 243–248.

[47] B. Fei, B. Qian, Z. Yang, R. Wang, W. C. Liu, C. L. Mak, J. H. Xin, *Carbon* **2008**, *46*, 1795–1797.

[48] P. Díaz, Y. Gimeno, P. Carro, S. González, P. L. Schilardi, G. Benítez, R. C. Salvarezza, A. H. Creus, *Langmuir* **2005**, *21*, 5924–5930.

[49] A. B. Mostert, B. J. Powell, I. R. Gentle, P. Meredith, *Appl. Phys. Lett.* **2012**, *100*, 093701.